RESEARCH ARTICLE

Capacitive Deionization

Energy & Environmental Materials WILEY

Rational Design of Titanium Carbide MXene Electrode Architectures for Hybrid Capacitive Deionization

S. Buczek, M. L. Barsoum, S. Uzun, N. Kurra, R. Andris, E. Pomerantseva, K. A. Mahmoud, and Y. Gogotsi

Intercalation redox materials have shown great promise for efficient water desalination due to available faradaic gallery sites. Symmetric capacitive deionization (CDI) cells previously demonstrated using MXenes were often limited in their salt adsorption capacity (SAC) and voltage window of operation. In this study, current collector- and binder-free $Ti_3C_2T_x$ MXene electrode architectures are designed with porous carbon as the positive electrode to demonstrate hybrid CDI (HCDI) operation. Furthermore, MXene current collectors are fabricated by employing a scalable doctor blade coating technique and subsequently spray coating a layer of a small flake MXene dispersion. Hydrophilic redox-active galleries of MXenes are capable of intercalating a variety of aqueous cations including Na^+, K^+, and Mg^{2+} ions, showing volumetric capacitances up to 250 F cm^{-3}. As a result, a salt removal capacity of 39 mg g^{-1} with decent cycling stability is achieved. This study opens new avenues for developing freestanding, binder- and additive-free MXene electrodes for HCDI applications.

1. Introduction

Clean and accessible water supply has become a global challenge due to population growth and industrial expansion.[1] Efficient and eco-friendly desalination techniques are becoming the most viable alternative to freshwater sources to secure an adequate global supply of potable water, especially in arid regions.[2,3] Traditional water purification technologies such as thermal distillation, reverse osmosis, and electrodialysis are promising but limited by their expensive infrastructure, high energy demand, and complexity of operation.[4] Unlike these industrial-sized systems that are bounded by locational constraints, capacitive deionization (CDI) is one of several technologies that has been shown to desalinate brackish water (water with 0.6–30 mg L^{-1} in total dissolved salts) on a laboratory bench scale.[5,6] CDI technology works by removing charged ionic impurities, taking advantage of capacitive effects under ambient conditions, with applied potentials (~1 V).[2-6]

Porous carbons are the most widely studied electrode materials for CDI, but they suffer from mediocre ion removal capacities (5–20 mg g^{-1}).[7] This is because traditional porous carbon and graphene electrodes exhibit a double-layer type charging mechanism predominantly, thus limited by the amount of surface sites and accessible pores for ion removal.[7] While low cost and high specific surface area have kept carbon as an attractive choice for energy storage applications, the rational design of a pore structure that can facilitate maximum penetration of ions could significantly improve the ion removal capacity and reversibility of porous carbon electrodes.[8] In an attempt to find materials that overcome these structural and charge saturation limitations, research beyond carbon into nanostructured transition metal compounds has shown great promise, due to the unique tunnel and layered architectures that these materials provide to host mobile ions.[9] Such materials are known as faradaic ion intercalation electrodes, which exploit redox behavior rather than a double-layer type of sorption to achieve high sorption capacities at high rates.[4] Hybrid CDI (HCDI) is the operating mode that arises from pairing a double-layer charging material with a faradaic ion intercalation material.[4,10] However, most transition metal oxides (*e.g.*, MnO_2, Co_3O_4) suffer from poor electronic conductivity, necessitating the fabrication of robust conductive electrodes for HCDI applications.[11] Two-dimensional (2D) nanomaterials offer slit type pores for accommodation of salt ions without undergoing volumetric changes, making them promising host materials for HCDI applications.[12,13] Moreover, faradaic intercalation materials, unlike porous carbons, are less prone to suffer from co-ion expulsion, hence may allow desalination of higher salinity water, including seawater. Lower co-ion expulsion might also simplify the system design, since incorporating ion exchange membranes would be noncompulsory.[4] The ideal electrode material for HCDI should have a high specific surface area, suitable pore structure, high redox activity, good electrical conductivity, and stability in aqueous electrolytes. These properties enable device operation at a high salt adsorption capacity (SAC) within a large voltage window of electrochemical stability with high reversibility and without corrosion.[3,4]

A large class of 2D transition metal carbides and nitrides (MXenes) that are hydrophilic and exhibit metallic conductivity have shown promise in high-rate pseudocapacitive energy storage applications.[14,15]

S. Buczek, M.L. Barsoum, S. Uzun, Dr. N. Kurra, R. Andris, Prof. E. Pomerantseva, Prof. Y. Gogotsi
Department of Materials Science and Engineering and A.J. Drexel Nanomaterials Institute, Drexel University, Philadelphia PA 19104, USA
E-mail: gogotsi@drexel.edu

K. A. Mahmoud
Qatar Environment and Energy Research Institute (QEERI), Hamad Bin Khalifa University (HBKU), P.O. Box 34110, Doha Qatar

The ORCID identification number(s) for the author(s) of this article can be found under https://doi.org/10.1002/eem2.12110.

DOI: 10.1002/eem2.12110

Usually, MXenes are synthesized from ternary layered ceramic materials such as MAX phases ($M_{n+1}AX_n$, where M is an early transition metal, A is an element from groups 13–16, X is carbon and/or nitrogen, and n = 1–4).[16-18] MXene synthesis involves selective etching of the A group element from its parent MAX phase, following an intercalation-assisted delamination.[19] The resulting MXene can be represented by the general formula, $M_{n+1}X_nT_x$, where T_x denotes the surface termination groups (-F, -Cl -O, and -OH), which are responsible for the hydrophilicity of MXenes.[19,20] MXenes have demonstrated a unique combination of 2D morphology and the ability to intercalate various cations spontaneously with subsequent surface redox reactions.[21,22] Since brackish water contains a mixture of dissolved salts (*e.g.*, NaCl, KCl, $MgCl_2$), MXene-based electrodes may be suitable for the electrochemical removal of these cations for wastewater treatments or water softening applications.[23] Additionally, their high electronic conductivity (10,000 S cm^{-1})[24] is the key for eliminating corrosive metal-based current collectors during CDI operation, a property that is unattainable by other 2D materials such as reduced graphene oxide (rGO) and MoS_2.[12] Additionally, the ability to use solution processing techniques with MXene dispersions, such as vacuum-assisted filtration and doctor blade coating methods, can potentially make conductive MXene coatings that can eliminate the use of external metal current collectors, thus reducing the electrode cost and process complexity.[24,25] Due to mixed surface terminations and large *d*-spacing (typically> 1.0 nm), MXenes are capable of electrosorbing ions over a wide potential window; however, there are two prevalent issues observed in literature.[26] The first is restacking of adjacent sheets due to van der Waals forces, a phenomenon common in MXenes and other 2D materials in general, causing restricted accessibility to electrochemically active sites for target applications. Researchers have tried to combat the effects of restacking by designing electrodes with more open architectures. Bao et al., developed porous freeze-dried $Ti_3C_2T_x$ MXene electrodes that showed improved SAC over restacked films for CDI.[27] Additionally, MXene electrodes are prone to oxidation under anodic potentials when operated in a symmetric cell configuration, eventually diminishing their cycling life.[28] HCDI cells employing porous carbon positive electrodes can help mitigate the stability issues of MXene electrodes as carbon can extend into the complementary anodic potentials of operation.

In this study, we demonstrated asymmetric MXene HCDI cells using activated carbon as the positive electrode for effective removal of salt ions (HCDI cell setup is shown in Figure S1, Supporting Information). We designed bi-stacked MXene electrodes, which consist of small and large $Ti_3C_2T_x$ MXene flakes. Small flakes offer shorter diffusion pathways and adsorption/intercalation of salt ions, while large flakes provide mechanical stability with conductive transport pathways. Moreover, the potential of MXene current collectors in HCDI applications is for the first time demonstrated by fabricating conductive MXene films using highly concentrated $Ti_3C_2T_x$ dispersions (48 mg mL^{-1}) via doctor blade coating method. These binder-free electrodes were found to have a SAC of 39 mg g^{-1} with 62% cycling stability over 25 CDI cycles. This work represents a major step toward exploring MXene-based architectures for HCDI applications.

2. Results and Discussion

Delaminated $Ti_3C_2T_x$ colloidal dispersion was prepared by the previously reported synthesis method as described in the Experimental Section. Manual agitation (or handshaking) during delamination results in large flakes (denoted as L-$Ti_3C_2T_x$), which can be further down-sized through probe sonication (denoted as S-$Ti_3C_2T_x$) as shown in **Figure 1**a. Typically, as-synthesized colloidal solutions are comprised of flakes with lateral sizes above 1 μm, while probe sonication reduces the flake sizes down to hundreds of nanometers (Figure 1b).[29] Due to the stable colloidal nature of MXenes in water, they can be easily processed as binder-free, flexible, freestanding films through vacuum-assisted filtration[19] and a blade coating method.[24] It is known that freestanding films composed of large flakes exhibit excellent electrical conductivity (at least 5000 S cm^{-1}, depending on the intrinsic electronic quality and lateral size of flakes resulting from different synthesis routes

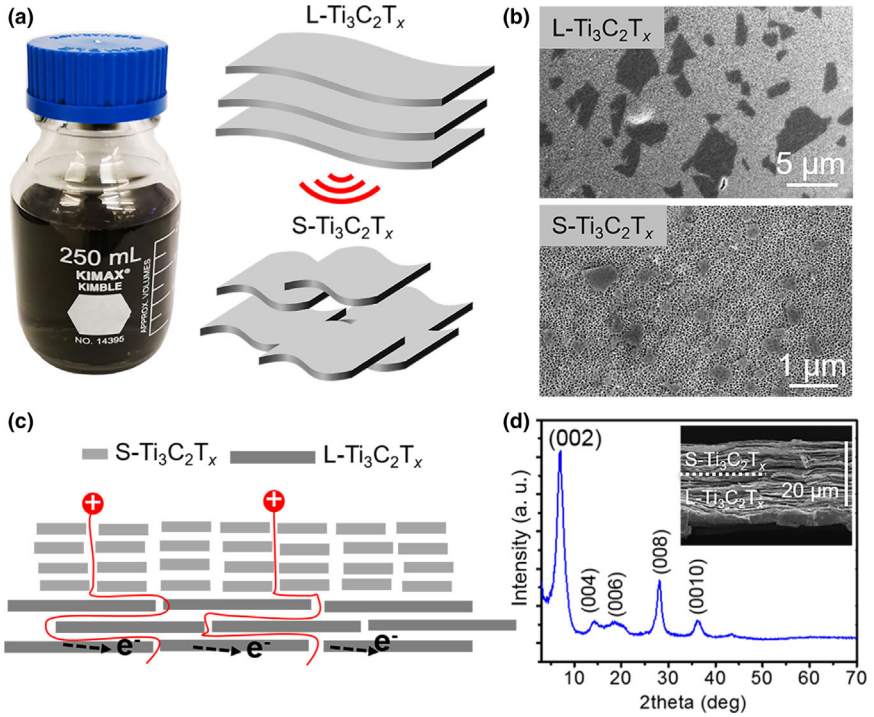

Figure 1. a) $Ti_3C_2T_x$ colloidal dispersion obtained through manual shaking to produce large flakes (L-$Ti_3C_2T_x$) and then reduced in size *via* probe sonication to produce small flakes (S-$Ti_3C_2T_x$). b) Corresponding SEM micrographs for L-$Ti_3C_2T_x$ (top) and S-$Ti_3C_2T_x$ (bottom) flakes. c) Schematic depicting ion diffusion paths across the L-$Ti_3C_2T_x$ and S-$Ti_3C_2T_x$ flakes in case of bi-stacked MXene films. d) X-ray diffraction pattern for the bi-stacked MXene film, where the inset shows the cross-sectional SEM image of representative bi-stacked MXene film.

as well as flake alignment), albeit suffering from poor ion transportation.[30] However, freestanding, vacuum-filtered films consisting of small flakes may appear brittle (with mediocre electronic conductivity) at the expense of improving the ion transportation. To fabricate MXene electrodes with enhanced electronic, ionic, and mechanical properties, we developed a bi-stacked $Ti_3C_2T_x$ MXene electrode architecture, where small flakes at the liquid–surface interface facilitate ion transport into the bulk of the electrode while large flakes at the bottom aid the electronic conduction, as shown in Figure 1c.

Vacuum-assisted filtration allows the single step, binder-free fabrication of MXene electrodes with small flakes filtered on top of large flakes. While the boundaries between small and large flakes with similar composition are not ultimately clear, the structure of the bi-stacked films appears to be more open compared to compact films composed of large flakes alone.[25] As shown in Figure 1d, typical 2θ value is found to be around 6.88°, corresponding to *d*-spacing of 12.84 Å, which is beneficial for lowering ion diffusion barriers across MXene galleries. The presence of higher (00l) reflections for bi-stacked films signifies the alignment among the MXene flakes.

To investigate the capacitive performance of $Ti_3C_2T_x$ electrodes, three-electrode static tests were performed in 1M NaCl electrolyte. Since the charge storage capacities of delaminated $Ti_3C_2T_x$ are superior to multilayer lamellas, delaminated MXene films produced *via* vacuum-assisted filtration were chosen for evaluation of the desalination performance. As an intercalating faradaic electrode material, $Ti_3C_2T_x$ has shown maximum charge storage capacities (450 F g^{-1}, 1V window) in protic electrolytes.[15] However, neutral electrolytes, such as NaCl, KCl, and $MgCl_2$, were used in static testing conditions to select the optimized electrode architecture for desalination purposes. As shown in **Figure 2**a, the L-$Ti_3C_2T_x$ electrode showed broad redox peaks close to 0V (*vs.* Ag/AgCl), possibly due to the spontaneous intercalation of hydrated Na^+-ions into 2D MXene galleries. At a scan rate of 100 mV s^{-1}, the CV shape deviates drastically due to ion diffusion limitations across long travel paths on these short timescales.

S-$Ti_3C_2T_x$ electrodes show rectangular profiles with broad redox peaks around 0 V (*vs.* Ag/AgCl). The current responses at the potential extremes appear to be sharp, which is an indication of the capacitive response of small flakes, as shown in Figure 2b. Moreover, bi-stacked

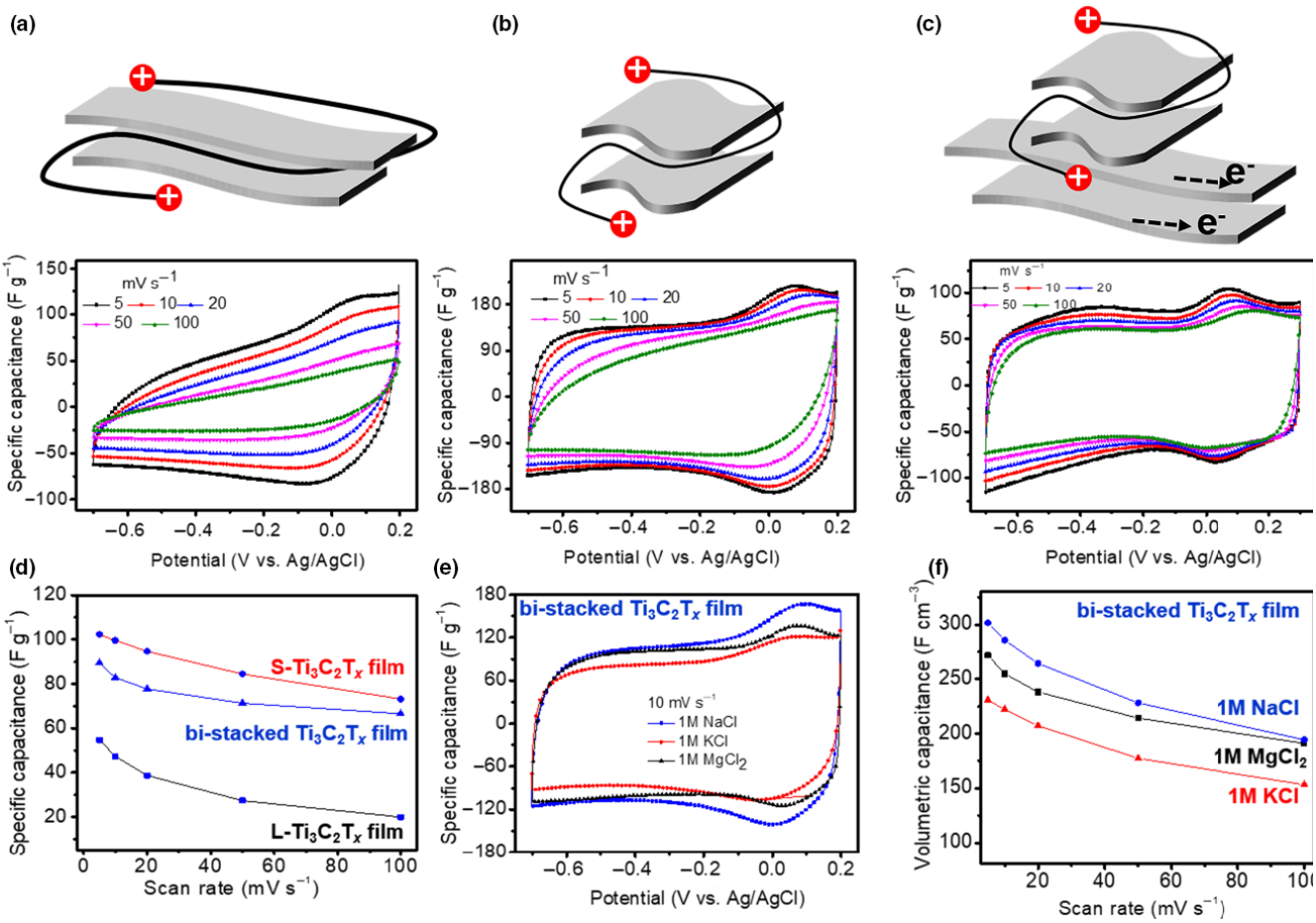

Figure 2. Comparison of electrochemical (static) performance of large (L-$Ti_3C_2T_x$), small (S-$Ti_3C_2T_x$), and bi-stacked MXene electrodes, produced using vacuum-assisted filtration in 1M NaCl electrolyte. Schematics depict the cations diffusion pathway across the large, small, and bi-stacked flakes. Cyclic voltammograms for a) L-$Ti_3C_2T_x$ electrodes, b) S-$Ti_3C_2T_x$ electrodes, and c) bi-stacked MXene electrodes at various scan rates in 1M NaCl. d) Specific capacitance versus scan rate for the MXene electrodes.e) Comparison of CVs at 10 mV s^{-1} for bi-stacked electrodes in 1M NaCl, 1M KCl, and 1M $MgCl_2$ electrolytes and corresponding f) rate handling plot, demonstrating volumetric capacitance change as a function of scan rate.

electrodes maintain a rectangular CV profile even at high scan rates as shown in Figure 2c, indicating excellent electrochemical behavior. The enhanced electrochemical performance could be explained by the dual contribution of large and small flakes, where both electronic and ionic conductivities are combined. The bi-stacked electrodes show both superior electrochemical rate performance over electrodes composed of only large or small MXene flakes. The S-$Ti_3C_2T_x$ electrode shows higher capacitance values compared to the L-$Ti_3C_2T_x$ and bi-stacked electrodes, likely due to higher amount of electrochemically accessible active sites, including edge sites. However, the bi-stacked MXene electrode possessed 90% of the absolute capacitance value of the S-$Ti_3C_2T_x$ electrode with a rate retention close to 74%.

Best-performing bi-stacked $Ti_3C_2T_x$ electrodes were tested in different chloride-based electrolytes with different cations such as Na^+, K^+, and Mg^{2+} as shown in Figure 2e. As expected, similar charge storage behavior is observed independent of the cation size. This is possibly attributed to the bi-stacked design, which is beneficial in accommodating a variety of cations with different charge densities. Volumetric capacitance for hydrated Na^+ ions is found to be around 300 F cm^{-3} at 5 mV s^{-1}, which is greater than the volumetric capacitances of hydrated K^+ (225 F cm^{-3}) and Mg^{2+} (270 F cm^{-3}) cations at the same scan rate. Moreover, the bi-stacked MXene electrodes retain up to 65% of their rate performance in 1M NaCl, 1M KCl, and 1M $MgCl_2$ electrolytes, as shown in Figure 2f. Due to the brittle nature of S-$Ti_3C_2T_x$ electrodes, further dynamic flow HCDI tests were conducted with large and bi-stacked $Ti_3C_2T_x$ electrodes while exploiting L-$Ti_3C_2T_x$ as a current collector.

MXene films produced via vacuum-assisted filtration (4 cm in diameter) were insufficiently large to accommodate the extended MXene contact and external connection (to the potentiostat) required for HCDI tests. Therefore, we used a scalable, blade coating method for fabricating MXene films using large flakes to achieve the minimum dimensions needed for HCDI cell assembly (0.8 cm width and 7 cm length). As shown in **Figure 3**a, L-$Ti_3C_2T_x$ dispersion was uniformly coated onto a glass bed using a doctor blade. After drying, double-sided Kapton tape was used to mechanically peel off MXene film from the glass bed. MXene dispersions containing probe-sonicated small flakes were then spray coated onto the MXene/Kapton tape current collector until a 10 μm thickness was achieved. Rolled activated carbon was employed as a positive electrode in HCDI cells. The static electrochemical performance of activated carbon electrodes was evaluated in 1M NaCl electrolyte as shown in Figure S2, Supporting Information.

The sodium ion removal performances of L-$Ti_3C_2T_x$ and bi-stacked electrodes are shown in Figure 3b. The concentration vs time curves exhibited by HCDI cells containing both types of electrodes illustrate consistent ion removal and ion release cycles, indicating the accessibility of 2D redox MXene galleries. Furthermore, the amplitudes of the cell containing the bi-stacked electrode are noticeably higher (Figure 3b). When normalized by the electrode mass, the bi-stacked electrode initially demonstrated higher ion removal capacity of 39.18 ± 1.73 mg g^{-1} over the first ten cycles than L-$Ti_3C_2T_x$ electrode (30.08 ± 0.99 mg g^{-1}) (Figure 3c). This result is higher than other HCDI studies using $Ti_3C_2T_x$ MXene electrodes that reported a capacity of 13 mg g^{-1} [22] and comparable to porous MXene films (45 mg g^{-1})[27] (see Table S1, Supporting Information).[31-36] The improved performance of the bi-stacked electrode at the start of cycling could be attributed to the higher initial porosity and accessibility of electrochemically active sites on the MXene surface and interlayer region, allowing for higher adsorption and intercalation of Na^+ ions being removed from solution, respectively. After 10 cycles, the performance of the bi-stacked electrode began to degrade and ion removal capacity dropped to 25.69 mg g^{-1}, similar to the value delivered by the L-$Ti_3C_2T_x$ electrode (28.64 mg g^{-1}) after 25 cycles (Figure 3c).

While smaller flakes may facilitate diffusion pathways, they might also introduce instability to the electrode structure. Figure 3d shows the XRD patterns of the bi-stacked electrode before cycling and after 25th ion release cycle. There is a primary (002) peak used to measure interlayer spacing, followed by higher (00l) reflections. It is important to note that the small flakes in the films made *via* doctor blade coating method exhibit a more compact layered structure (2θ ~ 7.48°) than films made using vacuum-assisted filtration (2θ ~ 6.88°).[24] However, these reflections at higher 2θ values are noticeably less intense after cycling, which indicate increased disorder in the film structure. This disorder could be the result of both the continuous flow of solution between the MXene layers and decreased flake overlap in the S-$Ti_3C_2T_x$ film compared to the L-$Ti_3C_2T_x$ film. The primary (002) peak is shifted to a smaller 2θ value after cycling. The increased interlayer spacing could be attributed to the entrapment of ions from solution within the interlayer region during cycling, thereby occupying interlayer sites and decreasing adsorption capacity. Similar structural and compositional dynamics have been reported for layered manganese oxide electrodes used for the removal of ions from water in HCDI cells.[37] The decrease in active volume

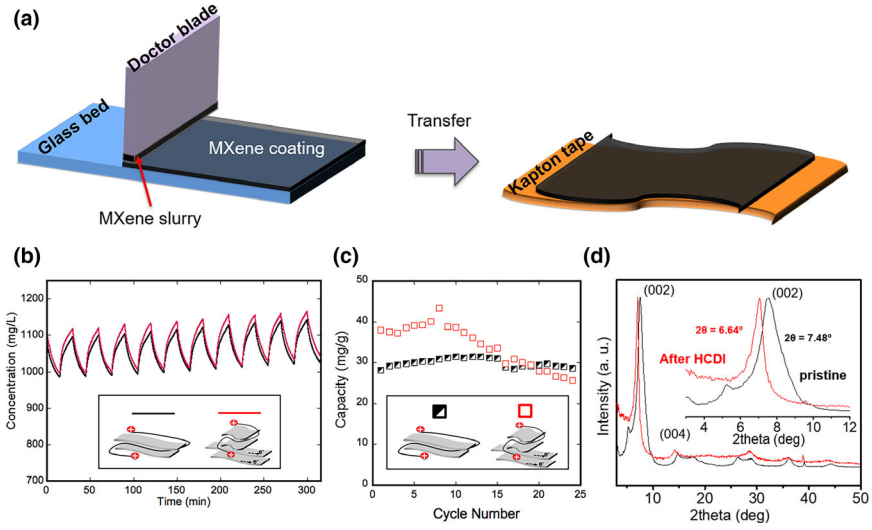

Figure 3. a) Schematic depicting the doctor blade coating method. L-$Ti_3C_2T_x$ MXene ink coated onto a glass bed followed by transfer to Kapton tape. Flow-based electrochemical performance of the L-$Ti_3C_2T_x$ and bi-stacked $Ti_3C_2T_x$ electrodes, including b) concentration versus time curves for the first 10 cycles, c) ion removal capacities (mg g^{-1}) through 25 cycles, and d) XRD patterns of the bi-stacked electrode before and after HCDI cycles. The post-cycling data were obtained after the 25th ion release step. The inset shows an expanded view of the (002) peak.

combined with the mechanical instability of the S-$Ti_3C_2T_x$ film can explain the degradation in removal capacity from 39 mg g^{-1} to 28 mg g^{-1} for the final 10 cycles of the bi-stacked electrode. Despite moderate capacity retention, the measured ion removal performance is still a notable achievement for CDI technology due to the binder-free MXene electrode acting as its own current collector. The mechanical integrity of the bi-stacked electrodes could be improved by pressing MXene films before cycling to assure that MXene flakes retain their original architecture. Highly porous MXene electrode architectures may be developed for flowable suspension electrodes in HCDI configuration.[38]

While this paper highlights some of the advantages of faradaic layered materials, like delaminated Ti_3C_2, over conventional porous carbon electrodes, stability remains a major issue in the former. It is almost inevitable that pristine MXene membranes will experience oxidation when operating in oxygen-saturated electrolytes like brackish water. Pairing MXene with porous carbon in an HCDI configuration instead of a symmetric configuration was done to limit the rate of oxidation (to potentially extend the cycling stability) of MXene as it operates comfortably in the negative potential window. Stability continues to be an important research direction for MXene materials in the context of sustainable CDI cell operation. Controlling surface chemistry as well as passivation of defect sites using polymers and surface protection coatings may be investigated toward developing stable MXene CDI cells.

3. Conclusion

In summary, current collector- and binder-free $Ti_3C_2T_x$ MXene electrode architectures were developed for HCDI applications. A bi-stacked MXene electrode design composed of small and large flakes that was employed to investigate the capacitive performance in a static 3-electrode configuration using a variety of aqueous electrolytes, including 1M solutions of NaCl, KCl, and $MgCl_2$. Volumetric capacitance up to 250 F cm^{-3} with a rate retention of 65% was achieved in the scan rate range of 5–100 mV s^{-1}. Furthermore, the design of a flowable HCDI system using MXene and porous carbon electrodes, operating at a voltage of +1.2 V for ions removal and a voltage of −1.2 V for ions release. The salt removal capacities up to 39 mg g^{-1} and cycling stability up to 25 cycles were demonstrated. This study opens avenues for developing MXene current collectors and new electrode architectures for sustainable HCDI systems to be used for water treatment applications.

4. Experimental Section

Synthesis of Delaminated $Ti_3C_2T_x$ MXene: All chemicals were used as-received without further purification. Layered ternary carbide Ti_3AlC_2 (MAX phase) powder was obtained from Carbon-Ukraine, Ltd. (particle size < 40 μm). $Ti_3C_2T_x$ MXene was synthesized by following the minimally intensive layer delamination (MILD) route, where selective etching of Al from Ti_3AlC_2 was achieved using *in situ* HF-forming etchant, as previously reported elsewhere.[19] The etching solution was prepared by adding 1 g of lithium fluoride (LiF, Alfa Aesar, 98+ %) to 20 mL of 9 M hydrochloric acid (HCl, Fisher, technical grade, 35-38%), followed by 5 minutes of stirring. 1 g of Ti_3AlC_2 powder was slowly added to the etchant solution at room temperature and continued stirring for 24 h at 600 rpm. The acidic suspension was washed with deionized (DI) water to a pH ≥ 6 *via* centrifugation at 3500 rpm (5 min per cycle) with subsequent decanting of the clear supernatant after each cycle. Around pH ≥ 6, a stable dark green supernatant of $Ti_3C_2T_x$ was observed and then collected after 30 min of centrifugation at 3500 rpm. The concentration of the $Ti_3C_2T_x$ solution was measured by filtering a specific amount of colloidal solution through a polypropylene filter (3501 Coated PP, Celgard LLC, Charlotte, NC), followed by drying under vacuum at 70 °C overnight. Large flakes of $Ti_3C_2T_x$ dispersed in water were probe-sonicated (Fisher Scientific model 505 Sonic Dismembrator, 500 W) for 20 minutes under pulse setting (8 s on pulse and 2 s off pulse) at an amplitude of 50% in an ice bath. Probe-sonicated $Ti_3C_2T_x$ solutions were centrifuged at 3500 rpm for 60 min, and the supernatant was collected.

Preparation of Freestanding $Ti_3C_2T_x$ MXene Film: To prepare freestanding $Ti_3C_2T_x$ films, two different methods were used: vacuum-assisted filtration and a blade coating method. To make a $Ti_3C_2T_x$ film *via* vacuum-assisted filtration, $Ti_3C_2T_x$ colloidal solutions of probe-sonicated, small flakes (S-$Ti_3C_2T_x$) or as-synthesized, large flakes (L-$Ti_3C_2T_x$) were filtered onto a Celgard membrane. Bi-stacked MXene films were made by sequentially filtering small flakes on top of a layer of large flakes using vacuum-assisted filtration. After the filtered film was dried in an ambient environment, the freestanding $Ti_3C_2T_x$ films were detached from the Celgard membrane and directly used as electrodes for static electrochemical measurements.

A blade coating method as shown in Figure 3 was used to prepare the large area MXene films for dynamic flow tests in a HCDI cell, as shown in our previous work.[24] Blade-coated $Ti_3C_2T_x$ films were prepared from highly concentrated $Ti_3C_2T_x$ dispersions (48 mg mL^{-1}) containing predominantly large MXene flakes. The height between the substrate and the blade edge has been fixed to 75 μm, 100 μm, and 200 μm, which corresponds to dry film thickness of 7 μm, 10 μm, and 18 μm, respectively. The blade-coated film with a thickness of 18 μm demonstrated an electrical conductivity of 10,800 S cm^{-1}.[39] Once the blade-coated film (thickness, 7 μm) was fully dried, S-$Ti_3C_2T_x$ MXene flakes (5 mg mL^{-1}) were spray coated onto the L-$Ti_3C_2T_x$ film surface until a thickness of 10 μm was achieved. Even though the blade-coated film with a maximum thickness of 18 μm demonstrated an electrical conductivity of 10,800 S cm^{-1}, the electrical conductivity of 5000 S cm^{-1} is sufficient for a current collector for CDI measurement. Once the blade-coated film was fully dried on the glass bed surface, double-sided Kapton tape was used to peel it off carefully.

Material Characterization: The X-ray diffraction (XRD) patterns were recorded by a powder diffractometer (Rigaku Smart Lab, USA) with Cu K_α radiation at a step size of 0.04° with 0.5 s dwelling time. The cross-section and the microstructure of the samples were characterized by a scanning electron microscope (SEM) (Zeiss Supra 50VP, Germany). The electrical conductivity of the samples was measured using a four-point probe (ResTest v1, Jandel Engineering Ltd., Bedfordshire, UK) with a probe distance of 1 mm.

Fabrication of Activated Carbon (AC) Films: Activated carbon (AC, YP50F grade) films were prepared by mixing 5 wt% polytetrafluoroethylene (60 wt% in water, Sigma-Aldrich) to 95 wt% of YP50F (Kuraray, Japan). The above slurry was rolled into 100 μm thick films followed by drying in a vacuum oven at 70 °C overnight. These AC

films were used as over-capacitive counter electrodes for static 3-electrode and HCDI tests under flow conditions.

Static Electrochemical Measurements (3-electrode measurements): The following electrochemical tests: cyclic voltammetry (CV), galvanostatic charge–discharge (GCD), and electrochemical impedance spectroscopy (EIS) were conducted at room temperature using a VMP3 electrochemical workstation (BioLogic, France). The 3-electrode measurements were performed in 1 M NaCl, 1M KCl, and 1M $MgCl_2$ electrolytes, in which $Ti_3C_2T_x$ electrodes (mass loading of 3.5–5.5 mg cm^{-2}, density ~ 3.3 g cm^{-3}) were employed as the working electrodes with over-capacitive activated carbon and Ag/AgCl (3 M KCl) as the counter and reference electrodes, respectively.

Gravimetric specific capacitance C_m (F g^{-1}) of electrode materials was calculated from the CV curves by integrating the discharge portion using the following equation:

$$C_m = \frac{1}{Vmv}\int i dV \quad (1)$$

where i is the current (mA), V is the potential window (V), v is the scan rate (mV s^{-1}), and m is the mass of the active material (mg).

$$\text{Areal capacitane, } C_A = C_m \times \text{mass loading } \left(\text{mg cm}^{-2}\right) \quad (2)$$

$$\text{Volumetric capacitance, } \quad C_V = C_A/\text{thickness} \quad (3)$$

Hybrid Capacitive Deionization Experiments (HCDI): Ion removal experiments were performed using a previously employed, custom-built HCDI cell shown schematically in Figure S1, Supporting Information.[9] The cell consisted of a Delrin exterior with the lid outfitted with hose connection nozzles for the pump tubing. Since activated carbon electrode (100 μm thick, ~645 mm^2, 100 mg) is not sufficiently conductive, it was attached to the bottom portion of the cell using a tin-coated current collector (3M). In contrast, the blade-coated L-$Ti_3C_2T_x$ MXene electrode (7 μm thick, ~340 mm^2, 15 mg) was adhered to the underside of the lid with the uncoated side of the Kapton tape, acting as its own current collector, due to its high electrical conductivity. Specifically, MXene flakes with large lateral dimensions, known to demonstrate efficient electron transport,[24] were used as current collector, which extended outside of the channel region for contacting with the potentiostat alligator connections (Figure S1 in Supporting Information). The carbon and MXene electrodes were covered by an anion and cation exchange membrane, respectively (AGC Engineering Co.). Finally, a Viton fluoroelastomer gasket with a 166 mm^3 flow channel and 3 nylon mesh spacers (Spectrum Laboratories, Inc.) were placed between the two electrodes to help mitigate the risk of a short circuit. After the cell was assembled, bolts at each corner were tightened to a force of 1 Newton to seal the cell, prevent leakage and promote good contact between the cell elements, while allowing salt solution to flow in the channel between the electrodes.

The HCDI cell was integrated with a Biologic VMP3 potentiostat and peristaltic pump. The pump cycled a 15 mL reservoir of 15 mM NaCl solution (Fisher Scientific) at approximately 20 mL min^{-1}. At the same time, 15 min ion removal and 15 min ion release half-cycles were generated by applying constant alternating potentials of 1.2 V and −1.2 V, respectively. Prior to the full 30 min cycles, five 10 min pre-cycles were performed to reach a dynamic steady-state condition.[29] A dip-in conductivity probe (eDAQ) was used to monitor the concentration of the NaCl solution reservoir, and conductivity measurements were converted to concentrations based on calibration curves generated in previous work.[9] Lastly, the ion removal capacity of the HCDI cell, measured in mg of salt per g of electrodes mass, was calculated using Equation 4.

$$\text{Ion Removal Capacity} = (\Delta C \times V)/M \quad (4)$$

where ΔC is the absolute difference between the maximum and minimum concentration (mg L^{-1}) during each respective cycle, V is the volume of NaCl solution (L), and M is the active mass of the electrodes normalized by the area of electrode in the flow channel (g), including binder and conductive additives when used for activated carbon.

This system demonstrates a proof-of-concept HCDI study employing a delaminated MXene electrode–current collector combination coupled with a carbon anode, operating under continuous flow. Upon polarizing electrodes, cations get adsorbed or trapped between slit pores with concurrent flow of desalinated water exiting the channel. The adsorbed or trapped ions are released back into the flow stream by reversing polarity of electrodes in the following discharge cycle. During the discharge cycle, concentrated salt solution (brine) flows out from the channel. In this continuous flow configuration, there was no separation of the purified and brine water streams. The concentration was measured continuously during cycling to observe the cycling stability of the system and interpret its longevity in real use. When implementing a more refined system for practical use, fresh water can be collected (in a separate vessel) in alternate cycles of operation by the method of polarizing electrodes to desalinate the water then using intentional bias reversal to regenerate the electrodes while finding other uses for the resulting brine solution.

Acknowledgements

Authors acknowledge the Materials Characterization Core (MCC) facility at Drexel University for providing access to characterization tools. Authors acknowledge the financial support from Qatar National Research Fund (a member of Qatar Foundation) through the NPRP Grant # 9-254-2-120. Support from the National Science Foundation (CMMI-1635233) is acknowledged toward endorsing the HCDI testing equipment. Authors thank Geetha Valurouthu for providing MXene samples.

Conflict of Interest

There are no conflicts of interest to declare.

Supporting Information

Supporting Information is available from the Wiley Online Library or from the author.

Keywords

MXene, bi-stacked design, water desalination, purification, CDI

Received: June 6, 2020
Revised: July 1, 2020
Published online: July 21, 2020

[1] C. J. Vörösmarty, P. B. McIntyre, M. O. Gessner, D. Dudgeon, A. Prusevich, P. Green, S. Glidden, S. E. Bunn, C. A. Sullivan, C. R. Liermann, P. M. Davies, *Nature* **2010**, *467*, 555.
[2] M. Pasta, C. D. Wessells, Y. Cui, F. La Mantia, *Nano Lett.* **2012**, *12*, 839.
[3] W. Tang, J. Liang, D. He, J. Gong, L. Tang, Z. Liu, D. Wang, G. Zeng, *Water Res.* **2019**, *150*, 225.
[4] P. Srimuk, X. Su, J. Yoon, D. Aurbach, V. Presser, *Nat. Rev. Mater.* **2020**, *5*, 517.
[5] M. A. Anderson, A. L. Cudero, J. Palma, *Electrochim. Acta* **2010**, *55*, 3845.
[6] M. E. Suss, S. Porada, X. Sun, P. M. Biesheuvel, J. Yoon, V. Presser, *Energy & Environ. Sci.* **2015**, *8*, 2296.
[7] P. Liu, T. Yan, L. Shi, H. S. Park, X. Chen, Z. Zhao, D. Zhang, *J. Mater. Chem. A* **2017**, *5*, 13907.
[8] S. Porada, L. Borchardt, M. Oschatz, M. Bryjak, J. S. Atchison, K. J. Keesman, S. Kaskel, P. M. Biesheuvel, V. Presser, *Energy Environ. Sci.* **2013**, *6*, 3700.
[9] B. W. Byles, D. A. Cullen, K. L. More, E. Pomerantseva, *Nano Energy* **2018**, *44*, 476.
[10] C. Zhang, D. He, J. Ma, W. Tang, T. D. Waite, *Water Res.* **2018**, *128*, 314.
[11] S. Porada, R. Zhao, A. van der Wal, V. Presser, P. M. Biesheuvel, *Prog. Mater Sci.* **2013**, *58*, 1388.
[12] K. Singh, S. Porada, H. D. de Gier, P. M. Biesheuvel, L. C. P. M. de Smet, *Desalination* **2019**, *455*, 115.
[13] E. Pomerantseva, F. Bonaccorso, X. Feng, Y. Cui, Y. Gogotsi, *Science* **2019**, *366*, eaan8285.
[14] B. Anasori, M. R. Lukatskaya, Y. Gogotsi, *Nat. Rev. Mater.* **2017**, *2*, 16098.
[15] M. R. Lukatskaya, S. Kota, Z. Lin, M.-Q. Zhao, N. Shpigel, M. D. Levi, J. Halim, P.-L. Taberna, M. W. Barsoum, P. Simon, Y. Gogotsi, *Nat. Energy* **2017**, *2*, 17105.
[16] G. Deysher, C. E. Shuck, K. Hantanasirisakul, N. C. Frey, A. C. Foucher, K. Maleski, A. Sarycheva, V. B. Shenoy, E. A. Stach, B. Anasori, Y. Gogotsi, *ACS Nano* **2020**, *14*, 204.
[17] Y. Gogotsi, B. Anasori, *ACS Nano* **2019**, *13*, 8491.
[18] B. Anasori, Y. Gogotsi, *2D Metal Carbides and Nitrides (MXenes), Structure, Properties and Applications*, Springer, Berlin **2019**.
[19] M. Alhabeb, K. Maleski, B. Anasori, P. Lelyukh, L. Clark, S. Sin, Y. Gogotsi, *Chem. Mater.* **2017**, *29*, 7633.
[20] M. Naguib, V. N. Mochalin, M. W. Barsoum, Y. Gogotsi, *Adv. Mater.* **2014**, *26*, 982.
[21] P. Srimuk, J. Halim, J. Lee, Q. Tao, J. Rosen, V. Presser, *ACS Sustainable Chem. Eng.* **2018**, *6*, 3739.
[22] P. Srimuk, F. Kaasik, B. Krüner, A. Tolosa, S. Fleischmann, N. Jäckel, M. C. Tekeli, M. Aslan, M. E. Suss, V. Presser, *J. Mater. Chem. A* **2016**, *4*, 18265.
[23] I. Ihsanullah, *Nano-Micro Lett.* **2020**, *12*, 72.
[24] C. J. Zhang, B. Anasori, A. Seral-Ascaso, S.-H. Park, N. McEvoy, A. Shmeliov, G. S. Duesberg, J. N. Coleman, Y. Gogotsi, V. Nicolosi, *Adv. Mater.* **2017**, *29*, 1702678.
[25] N. Kurra, M. Alhabeb, K. Maleski, C.-H. Wang, H. N. Alshareef, Y. Gogotsi, *ACS Energy Lett.* **2018**, *3*, 2094.
[26] J. Li, N. Kurra, M. Seredych, X. Meng, H. Wang, Y. Gogotsi, *Nano Energy* **2019**, *56*, 151.
[27] W. Bao, X. Tang, X. Guo, S. Choi, C. Wang, Y. Gogotsi, G. Wang, *Joule* **2018**, *2*, 778.
[28] J. Tang, T. S. Mathis, N. Kurra, A. Sarycheva, X. Xiao, M. N. Hedhili, Q. Jiang, H. N. Alshareef, B. Xu, F. Pan, Y. Gogotsi, *Angew. Chem. Int. Ed.* **2019**, *58*, 17849.
[29] K. Maleski, C. E. Ren, M.-Q. Zhao, B. Anasori, Y. Gogotsi, *ACS Appl. Mater. Interfaces* **2018**, *10*, 24491.
[30] Q. Jiang, N. Kurra, K. Maleski, Y. Lei, H. Liang, Y. Zhang, Y. Gogotsi, H. N. Alshareef, *Adv. Energy Mater.* **2019**, *9*, 1901061.
[31] P. M. Biesheuvel, R. Zhao, S. Porada, A. van der Wal, *J. Colloid Interface Sci.* **2011**, *360*, 239.
[32] J. Ma, Y. Cheng, L. Wang, X. Dai, F. Yu, *Chem. Eng. J.* **2020**, *384*, 123329.
[33] L. Agartan, K. Hantanasirisakul, S. Buczek, B. Akuzum, K. A. Mahmoud, B. Anasori, Y. Gogotsi, E. C. Kumbur, *Desalination* **2020**, *477*, 114267.
[34] A. Amiri, Y. Chen, C. Bee Teng, M. Naraghi, *Energy Storage Mater.* **2020**, *25*, 731.
[35] L. Guo, X. Wang, Z. Y. Leong, R. Mo, L. Sun, H. Y. Yang, *FlatChem* **2018**, *8*, 17.
[36] B. Chen, A. Feng, R. Deng, K. Liu, Y. Yu, L. Song, *A. C. S. Appl. Mater. Interfaces* **2020**, *12*, 13750.
[37] B. W. Byles, B. Hayes-Oberst, E. Pomerantseva, *ACS Appl. Mater. Interfaces* **2018**, *10*, 32313.
[38] C. Zhang, K. B. Hatzell, M. Boota, B. Dyatkin, M. Beidaghi, D. Long, W. Qiao, E. C. Kumbur, Y. Gogotsi, *Carbon* **2014**, *77*, 155.
[39] J. Zhang, N. Kong, S. Uzun, A. Levitt, S. Seyedin, P. A. Lynch, S. Qin, M. Han, W. Yang, J. Liu, X. Wang, Y. Gogotsi, J. M. Razal, *Adv. Mater.* **2020**, *32*, 2001093.

